

Dayside Clouds and an Elevated C/O Ratio in the Atmosphere of the Ultra-hot Jupiter WASP-19b

SUMAN SAHA ^{1,2} AND JAMES S. JENKINS ^{1,2}

¹*Instituto de Estudios Astrofísicos, Facultad de Ingeniería Ciencias, Universidad Diego Portales, Av. Ejército Libertador 441, Santiago, Chile*

²*Centro de Excelencia en Astrofísica y Tecnologías Afines (CATA), Camino El Observatorio 1515, Las Condes, Santiago, Chile*

(Accepted for publication in The Astronomical Journal)

ABSTRACT

Ultra-hot Jupiters (UHJs) offer exceptional opportunities for detailed atmospheric characterization via emission spectroscopy. We present a comprehensive analysis of the dayside atmosphere of WASP-19b—one of the shortest-period UHJs—using archival JWST NIRSpec/PRISM observations, leveraging its broad panchromatic wavelength coverage (0.6–5.2 μm). Using atmospheric retrievals, we report robust detections of H₂O (20.41 σ) and CO (4.79 σ), along with marginal evidence for CO₂ (2.11 σ) and VO (2.81 σ). Our retrievals also place strong constraints on the abundances of SiO and TiO, although their presence is not statistically confirmed. Furthermore, our analysis reveals strong evidence for clouds in this ultra-hot dayside atmosphere (4.3 σ), with indications of silicon dioxide (silica/quartz; SiO₂(s)) cloud formation—making WASP-19b the first UHJ with a statistically significant cloud detection. Leveraging the well-constrained molecular abundances, we infer a day-side C/O ratio of 0.77 ± 0.16 , a potentially super-solar value consistent with emerging trends among UHJs and suggestive of possible oxygen sequestration through cloud condensation. Our findings place WASP-19b as a key benchmark for modeling dayside atmospheric processes and evolutionary dynamics in extremely irradiated exoplanets.

1. INTRODUCTION

Emission spectroscopy of transiting exoplanets is rapidly emerging as one of the most powerful techniques for probing the physical structures and chemical compositions of their atmospheres. Ultra-hot Jupiters (UHJs)—gas giants with dayside temperatures exceeding 2000K—are particularly well-suited for such studies due to their strong thermal emission and inflated atmospheres (e.g., Mansfield et al. 2018; Coulombe et al. 2023; Ridden-Harper et al. 2023; Saha & Jenkins 2025a). Near-to mid-infrared emission spectra of these extreme worlds can reveal the precise atmospheric abundances of key molecular species—such as H₂O, CO, CO₂, and SiO—as well as place constraints on cloud composition and vertical structure (e.g., Inglis et al. 2024; Coulombe et al. 2025; Saha et al. 2025; Saha & Jenkins 2025a). Since UHJs may have formed through unique evolutionary pathways, such atmospheric characterization also offers valuable insights into their origins and dynamical histories (e.g., Mordasini et al. 2016; Brewer et al. 2017).

WASP-19b (Hebb et al. 2010), which was the shortest-period transiting exoplanet known at the time of its discovery, orbits its G8V-type host star in just ~ 0.79 days. With an equilibrium temperature of 2113K and a radius of $1.41 R_J$ (Cortés-Zuleta et al. 2020), it lies well within the UHJ population, orbiting the coolest host star among them all. These characteristics make WASP-19b a particularly compelling target for atmospheric follow-up studies. Several previous attempts have been made to characterize its atmosphere using both ground- and space-based observations, despite the challenge posed by its relatively faint host star ($V_{\text{mag}} \approx 12.25$).

Previous studies using HST and Spitzer have reported the detection of water vapor in the atmosphere of WASP-19b, along with the presence of hazes absorbing at shorter wavelengths (Tumborang et al. 2024; Edwards et al. 2023; Changeat et al. 2022; Wong et al. 2016; Huitson et al. 2013; Mandell et al. 2013; Anderson et al. 2013). Ground-based optical to near-infrared observations using VLT/FORS2, Magellan/IMACS, and VLT/ESPRESSO have also suggested the possible presence of TiO and reaffirmed the existence of high-altitude clouds and hazes (Sedaghati et al. 2017; Espinoza et al. 2019; Sedaghati et al. 2021). However, these earlier studies were unable to robustly constrain key chemical properties such as the metallicity or carbon-to-oxygen

(C/O) ratio, largely due to instrumental limitations and the relative faintness of the host star.

The C/O ratio has long been regarded as a key tracer of the formation and migration history of giant exoplanets (e.g., Öberg et al. 2011; Eistrup et al. 2018; Cridland et al. 2019). Super-solar C/O ratios inferred for several UHJs (Weiner Mansfield et al. 2024; Smith et al. 2024; Saha & Jenkins 2025a,b) are consistent with formation beyond the snow line followed by inward migration. However, accretion of inner protoplanetary dust and/or planetesimals is plausible during such migration scenarios and may alter or contaminate the observable atmospheric composition. The C/O ratio has also been proposed as a diagnostic for distinguishing between formation via core accretion and gravitational collapse (e.g., Madhusudhan et al. 2014; Bergin et al. 2024). In addition, oxygen depletion through sequestration into refractory condensates has been suggested as a mechanism that could artificially elevate the observed C/O ratios in gas-giant atmospheres (Fonte et al. 2023). Nonetheless, the relatively smaller number of such measurements currently limits the ability to robustly constrain formation pathways.

Robust estimation of the C/O ratio in planetary atmospheres requires precise measurements of the abundances of both carbon- and oxygen-bearing molecules. Since many of these species exhibit strong absorption features in the near- to mid-infrared, earlier ground-based instruments—limited both in sensitivity and spectral coverage in these wavelengths—have struggled to provide the necessary precision. The James Webb Space Telescope (JWST, Gardner et al. 2006), with its broad and high-precision spectroscopic coverage across this critical wavelength range, marks a major advancement. It enables the accurate detection of multiple key molecular species, thereby allowing unprecedented precision in the retrieval of atmospheric abundances, C/O ratios, and metallicities.

In this study, we present a comprehensive atmospheric characterization of the day side of the ultra-hot Jupiter WASP-19b, using archival panchromatic JWST emission spectroscopy obtained with NIRSpec/PRISM. Section 2 describes our methodology, including the data reduction, analyses and atmospheric modeling, while Section 3 presents the key results and discuss their broader implications.

2. METHODOLOGY

OBSERVATIONAL DATA

WASP-19b was observed by JWST during cycle 1 as part of the GTO program #1274 (PI: J Lunine). The observation, carried out on February 18, 2023, employed NIRSpec/PRISM (Jakobsen et al. 2022) in the Bright Object Time Series (BOTS; Espinoza et al. 2023) mode. This configuration enables low-resolution time-series spectroscopy across a broad wavelength range of $\sim 0.6\text{--}5.2\mu\text{m}$. The lower

spectral resolution can lead to saturation in moderately bright targets, making it unsuitable for many luminous sources. WASP-19b is relatively faint, which avoids immediate saturation, and allows broad wavelength coverage within a single transit. We accessed the publicly available data from the Barbara A. Mikulski Archive for Space Telescopes (MAST¹; doi: 10.17909/zya5-mg28). The observations span approximately 5.8 hours, covering the entire secondary eclipse of WASP-19b along with a substantial out-of-eclipse baseline. Full coverage of the secondary eclipse is essential for accurately modeling instrumental and astrophysical trends, particularly in high-precision emission spectroscopy.

DATA REDUCTION

The official JWST archive provides data at various calibration levels from the JWST Science Calibration Pipeline (Bushouse et al. 2022), ranging from stage 0 to stage 3. Stage 0 files contain the raw data in FITS format (“*uncal.fits”), which have four dimensions: detector columns, detector rows, the number of groups per integration, and the number of integrations per exposure. The data are divided into multiple sectors (three in our case) to accommodate their large volume. The observation uses 4 groups per integration and a total of 18231 integrations, providing exceptionally high cadence and high signal-to-noise (S/N) for time-series spectroscopy. The PRISM observations use the subarray SUB512, which has a spectral extent of 512 pixels on the NRS1 detector.

We reduced the stage 0 data using two independent pipelines: Eureka! (Bell et al. 2022) and exoTEDRF (formerly supreme-SPOON, Radica 2024). Both are well-established community pipelines, extensively validated (particularly Eureka!) through several previously published applications on JWST data (e.g., Alderson et al. 2023; Lustig-Yaeger et al. 2023; Powell et al. 2024; May et al. 2023 for Eureka! and Radica et al. 2024; Feinstein et al. 2023 for exoTEDRF). Using two independent reductions provides a cross-validation of the results, an important step in sensitivity-limited studies such as exoplanet atmospheric spectroscopy.

Both pipelines employ modular data reduction workflows that include key calibration and correction procedures—bias subtraction, flat-fielding, ramp fitting, and $1/f$ noise correction—followed by spectroscopic extraction of the time-series data. Calibration reference files were retrieved from the JWST Calibration Reference Data System (CRDS)². We closely followed the official documentation of both pipelines, adopting the recommended parameter settings and optimizations from our previous works (Saha & Jenkins 2025a,b).

¹ <https://mast.stsci.edu/>

² <https://jwst-crds.stsci.edu/>

The final extraction resulted in two-dimensional lightcurves resolved in both time and wavelength.

LIGHTCURVES MODELING

In contrast to the much higher resolution grisms, the NIR-Spec/PRISM observations are much more sparsely resolved in wavelength, and hence common binning practices used for grism observations are not optimal for these data. We have tested various binning schemes to compare the SNR of the lightcurves and the resulting planetary emission spectra, and found that even pixel level lightcurves have sufficiently high SNR to fit the secondary eclipses precisely. This is partly due to the fact that each PRISM pixel already covers a large enough wavelength range to deliver high-SNR data for relatively bright sources such as the host star WASP-19, and also because UHJs such as WASP-19b have substantially large secondary eclipse depths.

Therefore, we adopted pixel-level spectroscopic lightcurves for our analysis, which resulted in a total of 403 spectroscopic secondary eclipse lightcurves. This yields a significantly high effective resolution that allows us to distinguish between different molecular features, comparable to many grism-based studies in the literature, albeit at somewhat higher uncertainties and increased point-to-point scatter due to the lower overall brightness of the host star. However, because emission spectroscopic features from UHJs are expected to be among the most prominent planetary atmospheric signatures observable to date, the slightly larger uncertainties do not significantly affect our atmospheric interpretation.

To model the 1D lightcurves, we used our in-house pipeline, ExoELF (Exoplanets Lightcurves Fitter) (Saha et al. 2021; Saha & Sengupta 2021; Saha & Jenkins 2025a,b; Saha 2025). This pipeline integrates several open-source packages, including batman (Kreidberg 2015) for transit and eclipse modeling, emcee (Foreman-Mackey et al. 2013) and DYNESTY (Speagle 2020) for MCMC and nested sampling, respectively, and celerite (Foreman-Mackey et al. 2017; Foreman-Mackey 2018) and George (Ambikasaran et al. 2015) for Gaussian-process (GP) regression. ExoELF is optimized to handle large volumes of time-series data from HST and JWST observations, making it suitable for further applications as well.

Comparing the lightcurves from two independent reductions, we find that the exoTEDRF uncertainties remain effectively constant across large pixel ranges but exhibit pronounced, localized fluctuations. This is particularly noticeable in the pixel-level spectroscopic lightcurves (see Figure A1). Such behavior likely originates from computational approximations at certain stages of the reduction process, which also caused exoTEDRF uncertainties to be somewhat unreliable relative to those from Eureka!. In the white lightcurves,

the fluctuations strongly dominate the exoTEDRF uncertainties (see Figure A1). In contrast, the Eureka uncertainties appear consistent with the observed scatter in both spectroscopic and white lightcurves. For these reasons, we consider the Eureka! reduction to be more reliable and adopt it as the default dataset for our primary results.

We implemented a two-stage procedure to fit the lightcurves. In the first stage, we fit the white lightcurve with the mid-transit time, orbital parameters (scaled orbital semi-major axis and orbital inclination), eclipse depth, and detrending parameters free (see Table A1). In the second stage, we fit the spectroscopic lightcurves while fixing the mid-transit time and orbital parameters to the values obtained from the white lightcurve fit. This approach avoids poor constraints on wavelength-independent parameters in the lower-SNR spectroscopic lightcurves.

Proper detrending during lightcurve fitting is crucial to accurately estimate the secondary eclipse depths. We tested various detrending functions, from simple polynomials to GP regression. Because our lightcurves are mostly flat with only long-term trends, and the secondary eclipse signals have smaller amplitudes relative to the lightcurve SNRs—especially in spectroscopic lightcurves—complex detrending methods like GP regression tend to overfit and can misinterpret eclipse signals as trends. Similarly, very high-order polynomials can overfit the data. After testing several lower-order polynomials, we found that a fourth-order polynomial provides the best compromise, capturing both symmetric and asymmetric long-term trends. To ensure numerical stability, we used a fourth-order Legendre polynomial expansion instead of a standard polynomial, whose orthogonality mitigates correlations between higher-order terms.

Our combined lightcurve fits were performed using a nested sampling algorithm in DYNESTY. The emission spectra obtained from both independent reductions (see Figure 1) have a mean absolute difference of $\sim 1\sigma$, indicating excellent statistical agreement.

ATMOSPHERIC RETRIEVALS

Thanks to the high S/N of our extracted emission spectra, we performed a detailed atmospheric characterization using retrieval analyses. For this, we adopted petitRADTRANS (pRT, Mollière et al. 2019), a widely used and well-validated radiative transfer code in the exoplanet community (e.g., Kirk et al. 2024; Inglis et al. 2024; Louie et al. 2024; Petz et al. 2024; Blain et al. 2024). While pRT employs a one-dimensional radiative transfer framework, it is robust enough for the reliable interpretation of exoplanet spectra from current instruments such as JWST, offering nearly all functionalities needed for complex atmospheric analyses.

Our retrieval framework is based on the pRT retrieval routines (Nasedkin et al. 2024), which use PyMultinest (Feroz

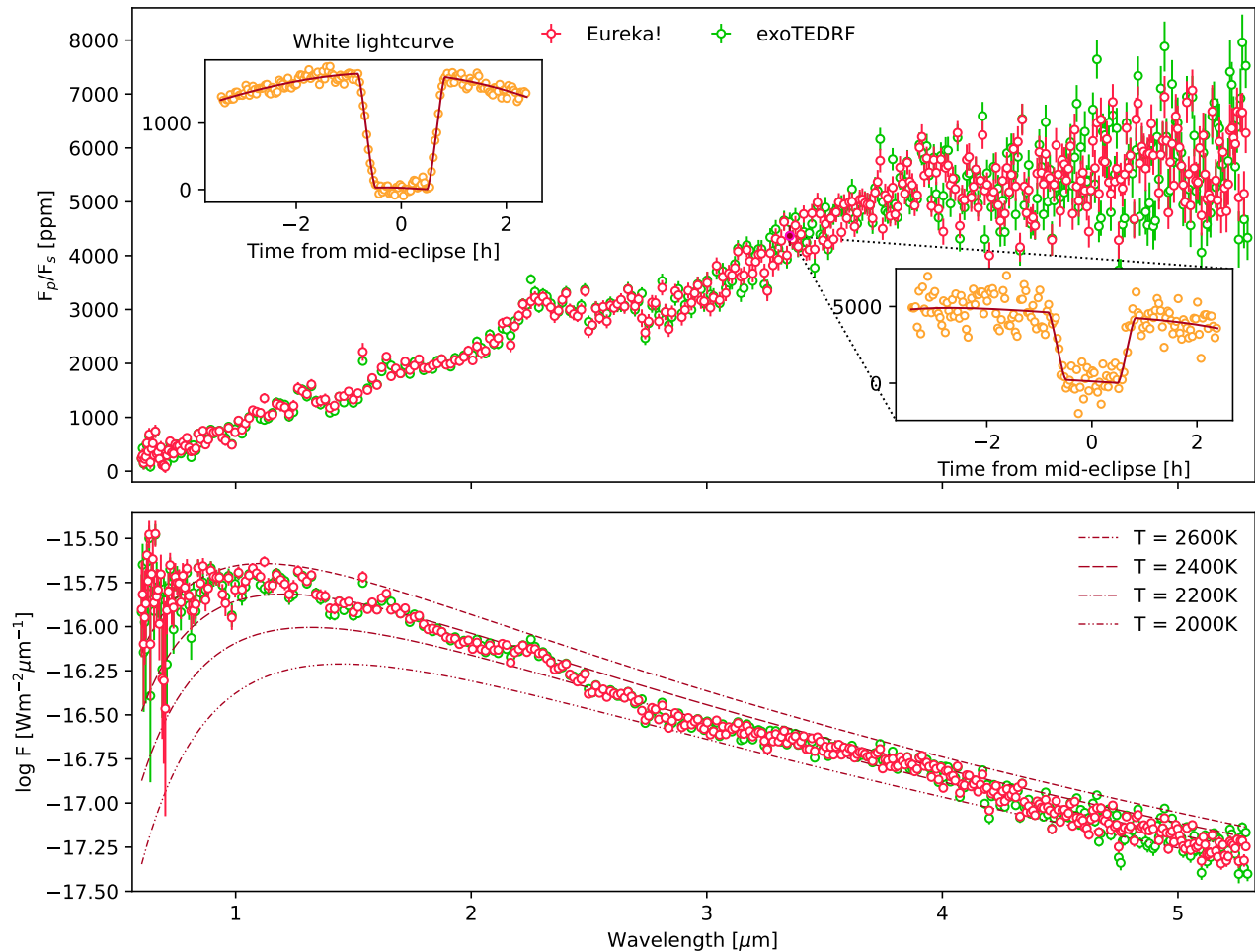


Figure 1. *Top:* Spectroscopic planet-to-star flux ratios with 1σ uncertainties, derived from two independent reductions of the NIRSPEC/PRISM data using Eureka! and exoTEDRF, followed by the modeling of the spectroscopic secondary eclipse lightcurves. The white lightcurve and the 196th spectroscopic lightcurve (Eureka!, both binned to 2-minute cadence for clarity) are shown along with their respective best-fit secondary-eclipse models. *Bottom:* Planetary emission spectra, normalized to the observer’s location, derived from the planet-to-star flux ratios above and modeled PHEONIX stellar spectrum. The mean absolute difference between the two independently reduced spectra is $\sim 1\sigma$, indicating excellent statistical consistency. For reference, blackbody curves corresponding to 2600K, 2400K, 2200K, and 2000K are also shown. The significant deviation of the planet’s spectra from blackbody expectations at shorter wavelengths is due to the dominating contribution of the reflected star-light by the planet.

et al. 2009; Buchner et al. 2014) for nested sampling of the posterior space. Given the high spectral resolution of our data, we adopted the line-by-line opacity mode with a model resolution of 20000, appropriate for such retrievals. The pressure-temperature (P–T) profile was parametrized following Guillot (2010), which provides sufficient flexibility without excessive computational cost. This parametrization involves four variables: the equilibrium (irradiation) temperature (T_{eq}), the internal temperature (T_{int}), the visible-to-infrared opacity ratio (γ), and the mean infrared opacity (κ_{IR}).

We applied both free and equilibrium chemistry models to describe the chemical abundances. In the free chemistry approach, the abundances of individual species (expressed as log-MMRs) were treated as vertically uniform free param-

eters, typically ranging between -14 and -0.2 (see Table A2). To improve computational efficiency, the upper bound was lowered for species not requiring a higher range in preliminary fits. For equilibrium chemistry, we used precomputed abundance tables from pRT, assuming chemical equilibrium at each pressure level.

Our models included opacities of all major molecules expected to contribute significantly across the observed wavelengths, including H_2O (Polyansky et al. 2018), CO (Rothman et al. 2010), CO_2 (Rothman et al. 2010), SiO (Barton et al. 2013), CH_4 (Hargreaves et al. 2020), HCN (Harris et al. 2006), C_2H_2 (Rothman et al. 2013), PH_3 (Sousa-Silva et al. 2015), H_2S (Rothman et al. 2013), TiO (Mollière et al. 2019), and VO (Mollière et al. 2019). Rayleigh scattering by

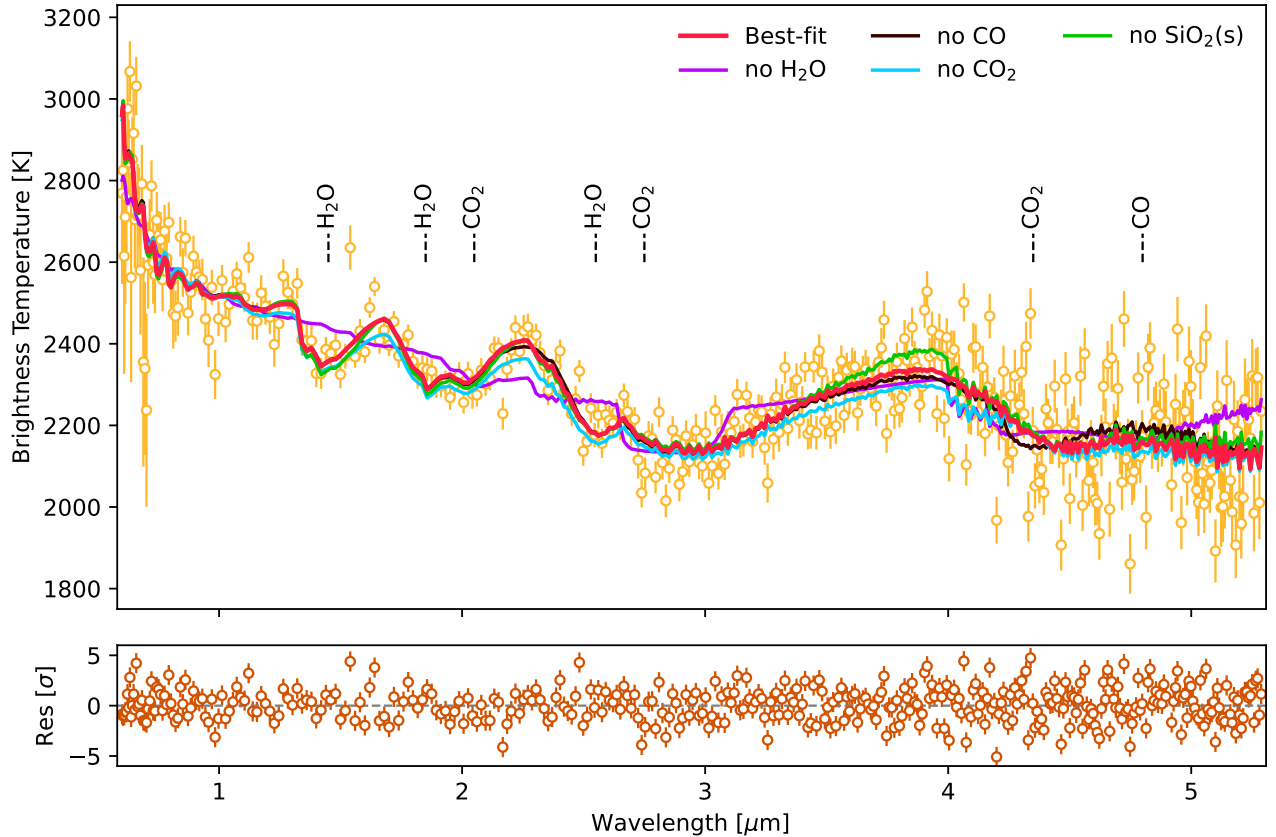


Figure 2. The observed emission spectrum of WASP-19b in terms of brightness temperatures (orange, Eureka!) is shown, along with the best-fit free-chemistry retrieved model and the residuals. Retrieved models excluding individual species are also shown, which were used to assess the statistical significance of their detection. Key spectral features from H₂O, CO, and CO₂, each detected with strong statistical significance, are also highlighted for reference.

H₂ (Dalgarno & Williams 1962) and He (Chan & Dalgarno 1965) and collision-induced absorption (CIA) from H₂-H₂ (Borysow et al. 2001; Borysow 2002) and H₂-He (Borysow et al. 1988, 1989) were included. Bound-free and free-free absorption by H⁻ (Gray 2008) was also considered, as it can be significant in ultra-hot Jupiter atmospheres.

We incorporated several condensate species expected to form clouds at these temperatures, following the formalism by Ackerman & Marley (2001), including MgSiO₃(s) (Jaeger et al. 1994; Ackerman & Marley 2001), Mg₂SiO₄(s) (Servoin & Piriou 1973; Costa et al. 2017), Al₂O₃(s) (Koike et al. 1995; Stull 1947), SiO₂(s) (Kitzmann & Heng 2018; Henning & Mutschke 1997; Koike et al. 1995; Stull 1947), TiO₂(s) (Kitzmann & Heng 2018; Zeidler et al. 2011; Posch et al. 2003; Siefke et al. 2016; Shornikov 2019), and CaTiO₃(s) (Kitzmann & Heng 2018; Posch et al. 2003; Ueda et al. 1998; Shornikov 2019). Their abundances at the cloud base were treated as free parameters in both free and equilibrium chemistry models. Additionally, we treated the sedimentation efficiency (fsed), the log-normal width of the particle size distribution (σ), the vertical eddy diffusion coefficient (kzz), and the cloud fraction (fc) as free parameters,

which together constrain the cloud profiles (Ackerman & Marley 2001). Finally, we included dayside scattering of starlight using a dayside averaged irradiance.

3. RESULTS AND DISCUSSION

The lower resolution of NIRSpec/PRISM enables high S/N observations for comparatively faint targets while providing exceptionally broad wavelength coverage $\sim 0.6\text{--}5.2\mu\text{m}$ from a single time-series observation. Moreover, due to their elevated temperatures and inflated radii, UHJs exhibit much stronger emission features than cooler exoplanets. Together, these factors make the emission spectra of WASP-19b ideally suited for precision retrieval analyses.

The free chemistry retrieval of the Eureka! spectrum yielded tightly constrained abundances of H₂O, CO, and CO₂, along with marginally constrained abundances for SiO, TiO, and VO (see Table 1, Figure 2 and A4). The retrieval also placed strong constraints on the cloud properties and the base abundance of SiO₂(s), indicating its presence. To assess the statistical significance (Kass & Raftery 1995) of each molecular detection, we performed additional retrievals excluding individual species from the model one

Table 1. Molecular abundances (in log-MMRs) and log-evidence from the atmospheric retrievals.

Model	[H ₂ O]	[CO]	[CO ₂]	[SiO]	[TiO]	[VO]	ln Z
Eureka! (free chem.)							
Best-fit	$-3.51^{+0.18}_{-0.13}$	$-2.8^{+0.38}_{-0.33}$	$-6.2^{+0.2}_{-0.24}$	$-4.21^{+0.72}_{-1.72}$	$-11.68^{+1.25}_{-1.3}$	$-8.92^{+0.21}_{-0.24}$	15535.29
No H ₂ O	–	$-0.83^{+0.07}_{-0.08}$	$-2.9^{+0.09}_{-0.08}$	$-0.77^{+0.07}_{-0.1}$	$-9.0^{+0.7}_{-0.54}$	$-8.7^{+0.5}_{-2.22}$	15327.07
No CO	$-3.69^{+0.12}_{-0.09}$	–	$-5.95^{+0.14}_{-0.11}$	$-8.38^{+2.18}_{-2.09}$	$-11.41^{+1.23}_{-1.37}$	$-9.02^{+0.27}_{-0.39}$	15523.80
No CO ₂	$-3.41^{+0.15}_{-0.14}$	$-2.37^{+0.29}_{-0.27}$	–	$-3.04^{+0.33}_{-0.31}$	$-11.86^{+1.22}_{-1.29}$	$-8.85^{+0.17}_{-0.21}$	15533.06
No SiO	$-3.5^{+0.17}_{-0.14}$	$-2.83^{+0.34}_{-0.35}$	$-6.1^{+0.21}_{-0.18}$	–	$-11.73^{+1.24}_{-1.22}$	$-8.89^{+0.21}_{-0.29}$	15537.23
No TiO	$-3.52^{+0.15}_{-0.13}$	$-2.83^{+0.32}_{-0.3}$	$-6.21^{+0.19}_{-0.25}$	$-4.26^{+0.69}_{-1.05}$	–	$-8.89^{+0.17}_{-0.17}$	15535.93
No VO	$-3.32^{+0.17}_{-0.15}$	$-2.37^{+0.28}_{-0.28}$	$-6.03^{+0.22}_{-0.28}$	$-3.65^{+0.47}_{-0.51}$	$-9.6^{+0.19}_{-0.18}$	–	15531.33
No clouds	$-3.45^{+0.18}_{-0.13}$	$-2.51^{+0.35}_{-0.28}$	$-6.33^{+0.3}_{-1.3}$	$-2.96^{+0.45}_{-0.46}$	$-10.84^{+0.96}_{-2.12}$	$-9.17^{+0.24}_{-1.14}$	15526.06
No SiO ₂ (s)	$-3.46^{+0.17}_{-0.13}$	$-2.49^{+0.34}_{-0.28}$	$-6.35^{+0.3}_{-1.48}$	$-2.95^{+0.47}_{-0.42}$	$-11.23^{+1.22}_{-1.85}$	$-9.15^{+0.22}_{-0.73}$	15527.58
Eureka! (eq. chem.)							
Best-fit	$-3.9^{+0.04}_{-0.04}$	$-2.29^{+0.03}_{-0.02}$	$-7.84^{+0.07}_{-0.07}$	$-3.74^{+0.05}_{-0.04}$	$-6.86^{+0.05}_{-0.05}$	$-9.21^{+0.06}_{-0.05}$	15528.51
No clouds	$-3.85^{+0.05}_{-0.04}$	$-2.37^{+0.04}_{-0.03}$	$-7.99^{+0.09}_{-0.08}$	$-3.75^{+0.04}_{-0.03}$	$-6.61^{+0.05}_{-0.04}$	$-8.88^{+0.06}_{-0.05}$	15497.91
exoTEDRF (free chem.)							
Best-fit	$-3.32^{+0.15}_{-0.14}$	$-2.59^{+0.28}_{-0.27}$	$-5.99^{+0.2}_{-0.24}$	$-3.78^{+0.62}_{-0.71}$	$-9.46^{+0.51}_{-0.37}$	$-9.78^{+0.79}_{-1.8}$	15500.30
No H ₂ O	–	$-0.72^{+0.13}_{-0.15}$	$-2.37^{+0.1}_{-0.12}$	$-1.16^{+0.28}_{-0.43}$	$-8.34^{+0.8}_{-1.5}$	$-8.25^{+0.74}_{-2.65}$	15500.30
No CO	$-3.14^{+0.24}_{-0.27}$	–	$-5.47^{+0.23}_{-0.25}$	$-7.84^{+2.23}_{-2.25}$	$-9.43^{+0.8}_{-1.14}$	$-9.13^{+0.56}_{-0.73}$	15493.46
No CO ₂	$-3.23^{+0.19}_{-0.15}$	$-2.12^{+0.35}_{-0.29}$	–	$-2.33^{+0.5}_{-0.44}$	$-9.69^{+0.41}_{-0.31}$	$-10.02^{+0.85}_{-2.03}$	15496.93
No SiO	$-3.24^{+0.21}_{-0.16}$	$-2.56^{+0.34}_{-0.32}$	$-5.81^{+0.22}_{-0.18}$	–	$-9.45^{+0.68}_{-0.68}$	$-9.24^{+0.57}_{-0.92}$	15502.49
No TiO	$-3.21^{+0.18}_{-0.16}$	$-2.39^{+0.34}_{-0.3}$	$-5.9^{+0.22}_{-0.32}$	$-3.54^{+0.66}_{-0.68}$	–	$-8.65^{+0.3}_{-0.26}$	15500.87
No VO	$-3.28^{+0.15}_{-0.14}$	$-2.45^{+0.33}_{-0.29}$	$-6.01^{+0.21}_{-0.35}$	$-3.41^{+0.69}_{-0.59}$	$-9.54^{+0.29}_{-0.21}$	–	15498.65
No clouds	$-3.23^{+0.23}_{-0.17}$	$-2.05^{+0.44}_{-0.35}$	$-6.45^{+0.51}_{-3.25}$	$-2.17^{+0.55}_{-0.52}$	$-9.92^{+0.21}_{-0.7}$	$-9.99^{+0.85}_{-2.39}$	15494.38
No SiO ₂ (s)	$-3.25^{+0.2}_{-0.15}$	$-2.08^{+0.4}_{-0.32}$	$-6.41^{+0.44}_{-3.18}$	$-2.22^{+0.52}_{-0.49}$	$-9.9^{+0.2}_{-0.46}$	$-10.25^{+0.88}_{-2.26}$	15496.16
exoTEDRF (eq. chem.)							
Best-fit	$-3.83^{+0.04}_{-0.05}$	$-2.26^{+0.05}_{-0.03}$	$-7.74^{+0.08}_{-0.07}$	$-3.64^{+0.1}_{-0.08}$	$-6.79^{+0.07}_{-0.06}$	$-9.14^{+0.07}_{-0.06}$	15493.25
No clouds	$-3.83^{+0.05}_{-0.04}$	$-2.35^{+0.04}_{-0.03}$	$-7.95^{+0.09}_{-0.08}$	$-3.73^{+0.04}_{-0.03}$	$-6.58^{+0.05}_{-0.04}$	$-8.84^{+0.07}_{-0.05}$	15455.61

at a time (see Table 1, Figure 2). From these comparisons, we find significant statistical evidence for the detection of H₂O (20.41 σ) and CO (4.79 σ), as well as marginal evidence for CO₂ (2.11 σ) and VO (2.81 σ). We found no statistically significant detection of SiO, although its abundance is well constrained from the retrievals. We also find no statistically significant detection of TiO despite a tight upper limit. We also find no evidence for contributions from H⁻ bound-free and free-free absorption opacities.

We also report statistically significant evidence for the presence of clouds (4.3 σ), with strong evidence for silicon dioxide (also called silica/quartz, SiO₂(s)) condensates (3.93 σ , see Table 1 and Figure 3). The contribution function shows strong features arising from the reflected star-light from the clouds at the shorter visible wavelengths, as well as gradually increasing emission features towards the longer wavelength end of the spectrum (see Figure 4). This makes WASP-19b the first UHJ with a statistically significant detection of clouds. We note that a parallel detection of condensate clouds (CaTiO₃(s)) has been reported by our team for WASP-121b (Saha & Jenkins 2025a), which can be considered as the second such detection, as also discussed in that work.

To independently verify these findings, we also performed analogous retrievals on the exoTEDRF spectrum, which yielded statistically consistent constraints on the molecular abundances (see Table 1 and Figure A7). Retrievals excluding specific species indicated significant statistical evidence for H₂O (21.29 σ) and CO (3.7 σ), along with marginal evidence for CO₂ (2.6 σ) and VO (1.82 σ), very similar to those obtained from the analysis of the Eureka! spectrum. Similarly, we find no statistically significant detection for SiO or TiO. The analysis also showed a consistent detection of clouds (3.44 σ), with strong evidence for SiO₂(s) condensates (2.88 σ).

Performing the equilibrium chemistry retrievals on the Eureka! spectrum, we found that the constrained molecular abundances were broadly consistent with those from the free chemistry retrievals (see Table 1, Figure 4, A5, and Figure A6). The only notable changes were a slightly elevated CO abundance and a much higher TiO abundance. The elevated CO abundance likely arises from the model attempting to maintain CO/H₂O ratios consistent with the pre-calculated abundance tables under chemical equilibrium. Similarly, the significantly higher TiO abundance likely arises from the pre-

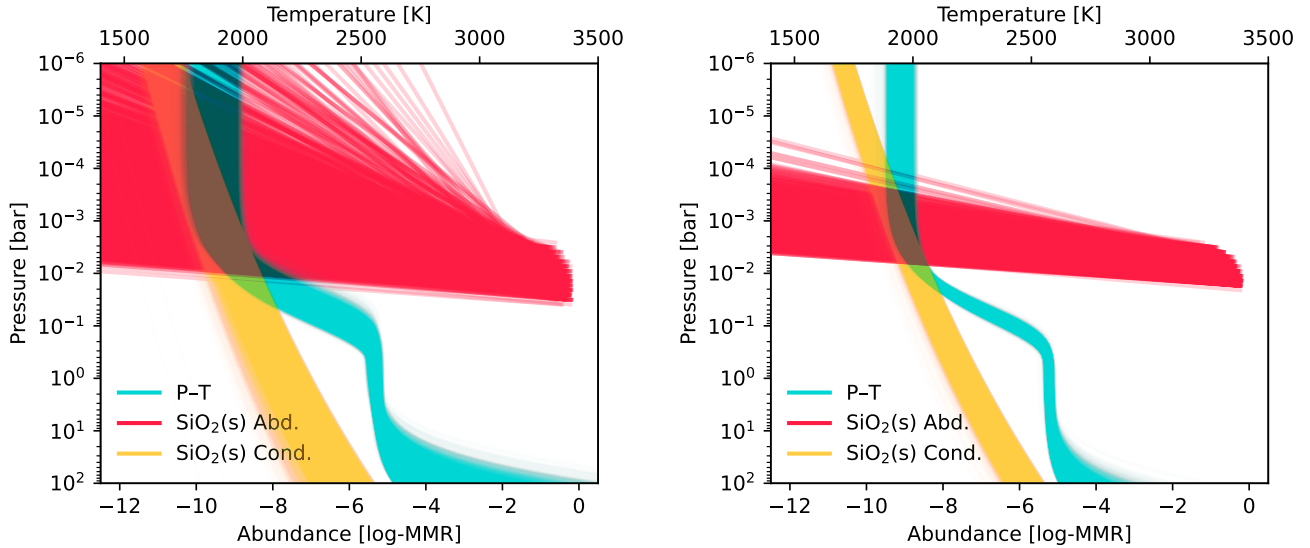


Figure 3. The retrieved posterior P–T profiles from the free (left) and equilibrium chemistry (right) retrievals of the Eureka! spectrum are shown, along with the corresponding SiO₂(s) condensation curves and their abundance profiles.

calculated equilibrium abundances expected at the retrieved temperatures, together with the well-constrained abundances of dominant species such as H₂O. While this may suggest a potential depletion of TiO relative to the expected equilibrium abundances at the retrieved temperatures, the absence of robust TiO detection renders this inference inconclusive.

It is also worth noting that the overall abundances of the molecular species and the pressure-temperature (P–T) profiles retrieved using the equilibrium chemistry models appear more precisely constrained, which is mainly due to the additional constraints imposed by the priors derived from the pre-computed tables (see Table 1 and Figure 3), and may therefore not fully reflect the true atmospheric conditions. This is further reflected in the fact that the retrieved best-fit model from the equilibrium chemistry retrieval is statistically 3.68 σ less significant than the free chemistry fit. Nonetheless, the equilibrium chemistry fit also indicated strong evidence for the presence of clouds (7.82 σ), further supporting our inference of clouds in this dayside atmosphere.

Leveraging the precisely constrained abundances of the dominant molecular species, which show statistically significant detections (H₂O, CO, and CO₂) from the free chemistry retrievals of the Eureka! spectrum, we derive a highly constrained atmospheric C/O ratio of 0.77 ± 0.16 . When we also include the retrieved abundance of SiO, which remains a statistical non-detection, we obtain a C/O ratio of 0.75 ± 0.17 , which is highly consistent with the former value. Similarly, using the retrieved abundances from the free chemistry modeling of the exoTEDRF spectrum, we obtained a C/O ratio of 0.78 ± 0.12 (0.75 ± 0.14 when including SiO), which is likewise highly consistent. This potentially super-solar C/O ratio in the dayside atmosphere of WASP-19b is consistent

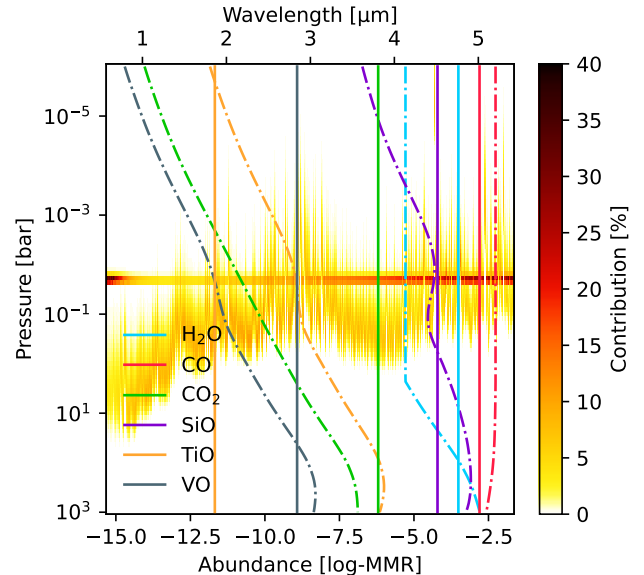


Figure 4. The retrieved median abundances of H₂O, CO, CO₂, SiO, TiO, and VO are shown from both free (solid) and equilibrium (dashed-dotted) retrievals for comparison (Eureka!), along with the median contribution function from the free chemistry retrievals. The strong contribution from SiO₂(s) cloud is apparent.

with the emerging trend of elevated C/O ratios reported in the recent studies of other UHJs using both JWST and non-JWST observations.

Given JWST’s capability to tightly constrain key molecular abundances, we compiled a literature sample of precisely measured C/O ratios for a broad population of exoplanets to examine possible population-level trends (Figure 5). The literature values were adopted from (Benneke et al. 2024;

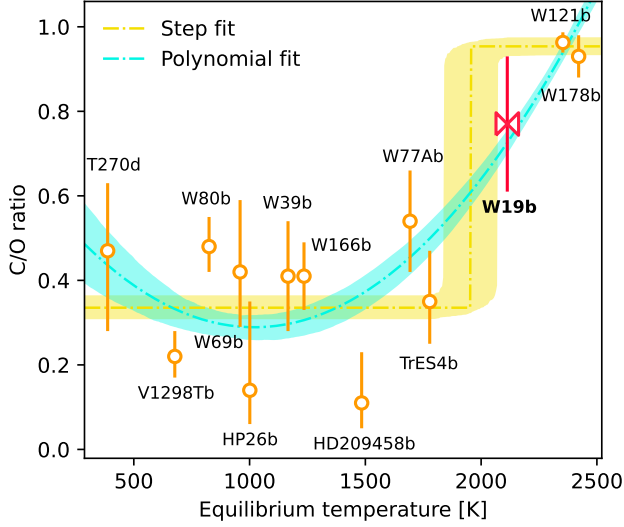


Figure 5. Several reported C/O ratios for a wide range of exoplanets based on JWST observations are shown, plotted against their equilibrium temperatures, with the estimated C/O ratio for WASP-19b from this work highlighted as the magenta bowtie. A step-function model illustrating the potential onset of super-solar C/O ratios in UHJs is shown, along with a quadratic polynomial model representing a gradual increase of the C/O ratio with equilibrium temperature, both with their corresponding 1σ uncertainties.

Weiner Mansfield et al. 2024; Xue et al. 2024; Edwards & Changeat 2024; Madhusudhan et al. 2011; Khorshid et al. 2024; Wisner et al. 2025; Meech et al. 2025; Gressier et al. 2025; Deka et al. 2025; Barat et al. 2025; Mayo et al. 2025; Saha & Jenkins 2025a,b), and several of the corresponding equilibrium temperatures were taken from (Saha 2023, 2024).

To investigate the potential onset of super-solar C/O ratios among the hottest exoplanets, we modeled the compiled C/O ratios using a step function fit (see Figure 5), obtaining $C/O_{\text{low}} = 0.34 \pm 0.03$, $C/O_{\text{high}} = 0.95 \pm 0.02$, and $T_{\text{break}} = 1953.2 \pm 111.5$ K. We also tested a scenario in which the C/O ratio gradually increases with equilibrium temperature by modeling the compiled C/O ratios using a quadratic polynomial function, $C/O = a_0 + a_1 T_{\text{eq}} + a_2 T_{\text{eq}}^2$ (see Figure 5), yielding $a_0 = 0.67 \pm 0.16$, $a_1 = -7.47 \times 10^{-4} \pm 2.38 \times 10^{-4}$, and $a_2 = 3.66 \times 10^{-7} \pm 7.43 \times 10^{-8}$.

Comparing both fits, we find that the step function fit provides a slightly better fit for the data than the quadratic polynomial model with $\Delta\text{BIC} = 2.75$. Although this evidence is weak, the comparison highlights a potential onset of highly elevated C/O ratios in UHJs. While the current dataset remains limited and many reported values have yet to be independently verified, these results suggest a possible transition toward super-solar C/O ratios at $T_{\text{eq}} \gtrsim 2000$ K. We emphasize, however, that a larger sample of uniformly analyzed targets will be essential to confirm and refine this apparent

trend. In particular, obtaining precise C/O measurements for additional UHJs and hot Jupiters near the transition region (~ 2000 K) will be critical for establishing the robustness of this trend and for improving our understanding of the underlying physical mechanisms.

Although super-solar C/O ratios in exoplanet atmospheres have previously been attributed to formation beyond the ice line followed by inward migration (e.g., Brewer et al. 2017; Schneider & Bitsch 2021), this mechanism alone cannot account for the highly elevated C/O values observed in UHJs. Many hot Jupiters are also believed to have formed at wide separations before migrating inward, yet they exhibit substantially lower C/O ratios. Instead, we hypothesize that the onset of extreme C/O ratios in UHJs originates from the sequestration of oxygen-bearing condensates on their nightsides (e.g., Fonte et al. 2023). The extremely high temperatures in UHJ dayside atmospheres act as a catalyst for this process by maintaining refractory species such as TiO and SiO in gaseous form. As these gases cool in the upper atmosphere, they condense into refractory cloud particles—such as $\text{SiO}_2(\text{s})$ in WASP-19b and $\text{CaTiO}_3(\text{s})$ in WASP-121b—which may then be advected to the nightside by strong atmospheric circulation. There, these condensates can rain or become cold-trapped, ultimately depleting the dayside of oxygen and leading to the observed enhancement in the C/O ratio.

Using the estimated molecular abundances from the free chemistry retrieval of the Eureka! spectrum, we inferred a metallicity of $0.2_{-0.1}^{+0.28} \times \text{solar}$. Although this value is sub-solar, the estimate is strongly driven by the most dominant molecule, CO, and therefore primarily reflects a slightly depleted CO abundance. This is also apparent when comparing the retrieved abundances with those from the equilibrium chemistry fit, and could be due to an overall depletion of oxygen in the dayside atmosphere. While any inference regarding formation mechanisms remains inconclusive based on this highly approximated metallicity, scenarios involving substantial mass loss due to photoevaporation can likely be ruled out.

We thank the anonymous reviewer for their constructive comments and suggestions, which have helped improve the manuscript. SS acknowledges Fondo Comité Mixto-ESO Chile ORP 025/2022 to support this research. The computations presented in this work were performed using the Geryon-3 supercomputing cluster, which was assembled and maintained using funds provided by the ANID-BASAL Center FB210003, Center for Astrophysics and Associated Technologies, CATA. This work is based [in part] on observations made with the NASA/ESA/CSA James Webb Space Telescope. The data were obtained from the Mikulski Archive for Space Telescopes at the Space Telescope Science Institute, which is operated by the Association of Universi-

ties for Research in Astronomy, Inc., under NASA contract NAS 5-03127 for JWST. These observations are associated with program #2055. JSJ gratefully acknowledges support

by FONDECYT grant 1240738 and from the ANID BASAL project FB210003.

REFERENCES

- Ackerman, A. S., & Marley, M. S. 2001, *ApJ*, 556, 872, doi: [10.1086/321540](https://doi.org/10.1086/321540)
- Alderson, L., Wakeford, H. R., Alam, M. K., et al. 2023, *Nature*, 614, 664, doi: [10.1038/s41586-022-05591-3](https://doi.org/10.1038/s41586-022-05591-3)
- Ambikasaran, S., Foreman-Mackey, D., Greengard, L., Hogg, D. W., & O’Neil, M. 2015, *IEEE Transactions on Pattern Analysis and Machine Intelligence*, 38, 252, doi: [10.1109/TPAMI.2015.2448083](https://doi.org/10.1109/TPAMI.2015.2448083)
- Anderson, D. R., Smith, A. M. S., Madhusudhan, N., et al. 2013, *MNRAS*, 430, 3422, doi: [10.1093/mnras/stt140](https://doi.org/10.1093/mnras/stt140)
- Barat, S., Désert, J.-M., Mukherjee, S., et al. 2025, *AJ*, 170, 165, doi: [10.3847/1538-3881/adec89](https://doi.org/10.3847/1538-3881/adec89)
- Barton, E. J., Yurchenko, S. N., & Tennyson, J. 2013, *MNRAS*, 434, 1469, doi: [10.1093/mnras/stt1105](https://doi.org/10.1093/mnras/stt1105)
- Bell, T., Ahrer, E.-M., Brande, J., et al. 2022, *The Journal of Open Source Software*, 7, 4503, doi: [10.21105/joss.04503](https://doi.org/10.21105/joss.04503)
- Benneke, B., Roy, P.-A., Coulombe, L.-P., et al. 2024, arXiv e-prints, arXiv:2403.03325, doi: [10.48550/arXiv.2403.03325](https://doi.org/10.48550/arXiv.2403.03325)
- Bergin, E. A., Booth, R. A., Colmenares, M. J., & Ilee, J. D. 2024, *ApJL*, 969, L21, doi: [10.3847/2041-8213/ad5839](https://doi.org/10.3847/2041-8213/ad5839)
- Blain, D., Landman, R., Mollière, P., & Dittmann, J. 2024, *A&A*, 690, A63, doi: [10.1051/0004-6361/202450767](https://doi.org/10.1051/0004-6361/202450767)
- Borysow, A. 2002, *A&A*, 390, 779, doi: [10.1051/0004-6361:20020555](https://doi.org/10.1051/0004-6361:20020555)
- Borysow, A., Frommhold, L., & Moraldi, M. 1989, *ApJ*, 336, 495, doi: [10.1086/167027](https://doi.org/10.1086/167027)
- Borysow, A., Jorgensen, U. G., & Fu, Y. 2001, *JQSRT*, 68, 235, doi: [10.1016/S0022-4073\(00\)00023-6](https://doi.org/10.1016/S0022-4073(00)00023-6)
- Borysow, J., Frommhold, L., & Birnbaum, G. 1988, *ApJ*, 326, 509, doi: [10.1086/166112](https://doi.org/10.1086/166112)
- Brewer, J. M., Fischer, D. A., & Madhusudhan, N. 2017, *AJ*, 153, 83, doi: [10.3847/1538-3881/153/2/83](https://doi.org/10.3847/1538-3881/153/2/83)
- Buchner, J., Georgakakis, A., Nandra, K., et al. 2014, *A&A*, 564, A125, doi: [10.1051/0004-6361/201322971](https://doi.org/10.1051/0004-6361/201322971)
- Bushouse, H., Eisenhamer, J., Dencheva, N., et al. 2022, *JWST Calibration Pipeline, 1.7.0*, Zenodo, doi: [10.5281/zenodo.7071140](https://doi.org/10.5281/zenodo.7071140)
- Chan, Y. M., & Dalgarno, A. 1965, *Proceedings of the Physical Society*, 85, 227, doi: [10.1088/0370-1328/85/2/304](https://doi.org/10.1088/0370-1328/85/2/304)
- Changeat, Q., Edwards, B., Al-Refaie, A. F., et al. 2022, *ApJS*, 260, 3, doi: [10.3847/1538-4365/ac5cc2](https://doi.org/10.3847/1538-4365/ac5cc2)
- Cortés-Zuleta, P., Rojo, P., Wang, S., et al. 2020, *A&A*, 636, A98, doi: [10.1051/0004-6361/201936279](https://doi.org/10.1051/0004-6361/201936279)
- Costa, G. C. C., Jacobson, N. S., & Fegley, Jr., B. 2017, *Icarus*, 289, 42, doi: [10.1016/j.icarus.2017.02.006](https://doi.org/10.1016/j.icarus.2017.02.006)
- Coulombe, L.-P., Benneke, B., Challener, R., et al. 2023, *Nature*, 620, 292, doi: [10.1038/s41586-023-06230-1](https://doi.org/10.1038/s41586-023-06230-1)
- Coulombe, L.-P., Radica, M., Benneke, B., et al. 2025, *Nature Astronomy*, doi: [10.1038/s41550-025-02488-9](https://doi.org/10.1038/s41550-025-02488-9)
- Cridland, A. J., van Dishoeck, E. F., Alessi, M., & Pudritz, R. E. 2019, *A&A*, 632, A63, doi: [10.1051/0004-6361/201936105](https://doi.org/10.1051/0004-6361/201936105)
- Dalgarno, A., & Williams, D. A. 1962, *ApJ*, 136, 690, doi: [10.1086/147428](https://doi.org/10.1086/147428)
- Deka, T., Majumdar, L., Basra Khan, T., et al. 2025, arXiv e-prints, arXiv:2510.27223, doi: [10.48550/arXiv.2510.27223](https://doi.org/10.48550/arXiv.2510.27223)
- Edwards, B., & Changeat, Q. 2024, *ApJL*, 962, L30, doi: [10.3847/2041-8213/ad2000](https://doi.org/10.3847/2041-8213/ad2000)
- Edwards, B., Changeat, Q., Tsiaras, A., et al. 2023, *ApJS*, 269, 31, doi: [10.3847/1538-4365/ac9f1a](https://doi.org/10.3847/1538-4365/ac9f1a)
- Eistrup, C., Walsh, C., & van Dishoeck, E. F. 2018, *A&A*, 613, A14, doi: [10.1051/0004-6361/201731302](https://doi.org/10.1051/0004-6361/201731302)
- Espinoza, N., Rackham, B. V., Jordán, A., et al. 2019, *MNRAS*, 482, 2065, doi: [10.1093/mnras/sty2691](https://doi.org/10.1093/mnras/sty2691)
- Espinoza, N., Úbeda, L., Birkmann, S. M., et al. 2023, *PASP*, 135, 018002, doi: [10.1088/1538-3873/aca3d3](https://doi.org/10.1088/1538-3873/aca3d3)
- Feinstein, A. D., Radica, M., Welbanks, L., et al. 2023, *Nature*, 614, 670, doi: [10.1038/s41586-022-05674-1](https://doi.org/10.1038/s41586-022-05674-1)
- Feroz, F., Hobson, M. P., & Bridges, M. 2009, *MNRAS*, 398, 1601, doi: [10.1111/j.1365-2966.2009.14548.x](https://doi.org/10.1111/j.1365-2966.2009.14548.x)
- Fonte, S., Turrini, D., Pacetti, E., et al. 2023, *MNRAS*, 520, 4683, doi: [10.1093/mnras/stad245](https://doi.org/10.1093/mnras/stad245)
- Foreman-Mackey, D. 2018, *Research Notes of the American Astronomical Society*, 2, 31, doi: [10.3847/2515-5172/aaaf6c](https://doi.org/10.3847/2515-5172/aaaf6c)
- Foreman-Mackey, D., Agol, E., Ambikasaran, S., & Angus, R. 2017, *AJ*, 154, 220, doi: [10.3847/1538-3881/aa9332](https://doi.org/10.3847/1538-3881/aa9332)
- Foreman-Mackey, D., Hogg, D. W., Lang, D., & Goodman, J. 2013, *PASP*, 125, 306, doi: [10.1086/670067](https://doi.org/10.1086/670067)
- Gardner, J. P., Mather, J. C., Clampin, M., et al. 2006, *SSRv*, 123, 485, doi: [10.1007/s11214-006-8315-7](https://doi.org/10.1007/s11214-006-8315-7)
- Gray, D. F. 2008, *The Observation and Analysis of Stellar Photospheres* (Cambridge University Press)
- Gressier, A., Batalha, N. E., Wogan, N., et al. 2025, *AJ*, 170, 292, doi: [10.3847/1538-3881/ae0929](https://doi.org/10.3847/1538-3881/ae0929)
- Guillot, T. 2010, *A&A*, 520, A27, doi: [10.1051/0004-6361/200913396](https://doi.org/10.1051/0004-6361/200913396)
- Hargreaves, R. J., Gordon, I. E., Rey, M., et al. 2020, *ApJS*, 247, 55, doi: [10.3847/1538-4365/ab7a1a](https://doi.org/10.3847/1538-4365/ab7a1a)

- Harris, G. J., Tennyson, J., Kaminsky, B. M., Pavlenko, Y. V., & Jones, H. R. A. 2006, *MNRAS*, 367, 400, doi: [10.1111/j.1365-2966.2005.09960.x](https://doi.org/10.1111/j.1365-2966.2005.09960.x)
- Hebb, L., Collier-Cameron, A., Triaud, A. H. M. J., et al. 2010, *ApJ*, 708, 224, doi: [10.1088/0004-637X/708/1/224](https://doi.org/10.1088/0004-637X/708/1/224)
- Henning, T., & Mutschke, H. 1997, *A&A*, 327, 743
- Huitson, C. M., Sing, D. K., Pont, F., et al. 2013, *MNRAS*, 434, 3252, doi: [10.1093/mnras/stt1243](https://doi.org/10.1093/mnras/stt1243)
- Inglis, J., Batalha, N. E., Lewis, N. K., et al. 2024, *ApJL*, 973, L41, doi: [10.3847/2041-8213/ad725e](https://doi.org/10.3847/2041-8213/ad725e)
- Jaeger, C., Mutschke, H., Begemann, B., Dorschner, J., & Henning, T. 1994, *A&A*, 292, 641
- Jakobsen, P., Ferruit, P., Alves de Oliveira, C., et al. 2022, *A&A*, 661, A80, doi: [10.1051/0004-6361/202142663](https://doi.org/10.1051/0004-6361/202142663)
- Kass, R. E., & Raftery, A. E. 1995, *Journal of the American Statistical Association*, 90, 773, doi: [10.1080/01621459.1995.10476572](https://doi.org/10.1080/01621459.1995.10476572)
- Khorshid, N., Min, M., Polman, J., & Waters, L. B. F. M. 2024, *A&A*, 685, A64, doi: [10.1051/0004-6361/202347124](https://doi.org/10.1051/0004-6361/202347124)
- Kirk, J., Ahrer, E.-M., Claringbold, A. B., et al. 2024, arXiv e-prints, arXiv:2410.08116, doi: [10.48550/arXiv.2410.08116](https://doi.org/10.48550/arXiv.2410.08116)
- Kitzmann, D., & Heng, K. 2018, *MNRAS*, 475, 94, doi: [10.1093/mnras/stx3141](https://doi.org/10.1093/mnras/stx3141)
- Koike, C., Kaito, C., Yamamoto, T., et al. 1995, *Icarus*, 114, 203, doi: [10.1006/icar.1995.1055](https://doi.org/10.1006/icar.1995.1055)
- Kreidberg, L. 2015, *PASP*, 127, 1161, doi: [10.1086/683602](https://doi.org/10.1086/683602)
- Louie, D. R., Mullens, E., Alderson, L., et al. 2024, arXiv e-prints, arXiv:2412.03675, doi: [10.48550/arXiv.2412.03675](https://doi.org/10.48550/arXiv.2412.03675)
- Lustig-Yaeger, J., Fu, G., May, E. M., et al. 2023, *Nature Astronomy*, 7, 1317, doi: [10.1038/s41550-023-02064-z](https://doi.org/10.1038/s41550-023-02064-z)
- Madhusudhan, N., Amin, M. A., & Kennedy, G. M. 2014, *ApJL*, 794, L12, doi: [10.1088/2041-8205/794/1/L12](https://doi.org/10.1088/2041-8205/794/1/L12)
- Madhusudhan, N., Harrington, J., Stevenson, K. B., et al. 2011, *Nature*, 469, 64, doi: [10.1038/nature09602](https://doi.org/10.1038/nature09602)
- Mandell, A. M., Haynes, K., Sinukoff, E., et al. 2013, *ApJ*, 779, 128, doi: [10.1088/0004-637X/779/2/128](https://doi.org/10.1088/0004-637X/779/2/128)
- Mansfield, M., Bean, J. L., Line, M. R., et al. 2018, *AJ*, 156, 10, doi: [10.3847/1538-3881/aac497](https://doi.org/10.3847/1538-3881/aac497)
- May, E. M., MacDonald, R. J., Bennett, K. A., et al. 2023, *ApJL*, 959, L9, doi: [10.3847/2041-8213/ad054f](https://doi.org/10.3847/2041-8213/ad054f)
- Mayo, A. W., Fortenbach, C. D., Louie, D. R., et al. 2025, *AJ*, 170, 50, doi: [10.3847/1538-3881/adda2e](https://doi.org/10.3847/1538-3881/adda2e)
- Meech, A., Claringbold, A. B., Ahrer, E.-M., et al. 2025, *MNRAS*, 539, 1381, doi: [10.1093/mnras/staf530](https://doi.org/10.1093/mnras/staf530)
- Mollière, P., Wardenier, J. P., van Boekel, R., et al. 2019, *A&A*, 627, A67, doi: [10.1051/0004-6361/201935470](https://doi.org/10.1051/0004-6361/201935470)
- Mordasini, C., van Boekel, R., Mollière, P., Henning, T., & Benneke, B. 2016, *ApJ*, 832, 41, doi: [10.3847/0004-637X/832/1/41](https://doi.org/10.3847/0004-637X/832/1/41)
- Nasedkin, E., Mollière, P., & Blain, D. 2024, *The Journal of Open Source Software*, 9, 5875, doi: [10.21105/joss.05875](https://doi.org/10.21105/joss.05875)
- Öberg, K. I., Murray-Clay, R., & Bergin, E. A. 2011, *ApJL*, 743, L16, doi: [10.1088/2041-8205/743/1/L16](https://doi.org/10.1088/2041-8205/743/1/L16)
- Petz, S., Johnson, M. C., Asnodkar, A. P., et al. 2024, *MNRAS*, 527, 7079, doi: [10.1093/mnras/stad3481](https://doi.org/10.1093/mnras/stad3481)
- Polyansky, O. L., Kyuberis, A. A., Zobov, N. F., et al. 2018, *MNRAS*, 480, 2597, doi: [10.1093/mnras/sty1877](https://doi.org/10.1093/mnras/sty1877)
- Posch, T., Kerschbaum, F., Fabian, D., et al. 2003, *ApJS*, 149, 437, doi: [10.1086/379167](https://doi.org/10.1086/379167)
- Powell, D., Feinstein, A. D., Lee, E. K. H., et al. 2024, *Nature*, 626, 979, doi: [10.1038/s41586-024-07040-9](https://doi.org/10.1038/s41586-024-07040-9)
- Radica, M. 2024, *The Journal of Open Source Software*, 9, 6898, doi: [10.21105/joss.06898](https://doi.org/10.21105/joss.06898)
- Radica, M., Coulombe, L.-P., Taylor, J., et al. 2024, *ApJL*, 962, L20, doi: [10.3847/2041-8213/ad20e4](https://doi.org/10.3847/2041-8213/ad20e4)
- Ridden-Harper, A., de Mooij, E., Jayawardhana, R., et al. 2023, *AJ*, 165, 211, doi: [10.3847/1538-3881/acc654](https://doi.org/10.3847/1538-3881/acc654)
- Rothman, L. S., Gordon, I. E., Barber, R. J., et al. 2010, *JQSRT*, 111, 2139, doi: [10.1016/j.jqsrt.2010.05.001](https://doi.org/10.1016/j.jqsrt.2010.05.001)
- Rothman, L. S., Gordon, I. E., Babikov, Y., et al. 2013, *JQSRT*, 130, 4, doi: [10.1016/j.jqsrt.2013.07.002](https://doi.org/10.1016/j.jqsrt.2013.07.002)
- Saha, S. 2023, *ApJS*, 268, 2, doi: [10.3847/1538-4365/acdb6b](https://doi.org/10.3847/1538-4365/acdb6b)
- , 2024, *ApJS*, 274, 13, doi: [10.3847/1538-4365/ad6a60](https://doi.org/10.3847/1538-4365/ad6a60)
- , 2025, *MNRAS*, 539, 928, doi: [10.1093/mnras/staf550](https://doi.org/10.1093/mnras/staf550)
- Saha, S., Chakrabarty, A., & Sengupta, S. 2021, *AJ*, 162, 18, doi: [10.3847/1538-3881/ac01dd](https://doi.org/10.3847/1538-3881/ac01dd)
- Saha, S., & Jenkins, J. S. 2025a, *ApJL*, 994, L39, doi: [10.3847/2041-8213/ae1c1c](https://doi.org/10.3847/2041-8213/ae1c1c)
- , 2025b, arXiv e-prints, arXiv:2510.11479, doi: [10.48550/arXiv.2510.11479](https://doi.org/10.48550/arXiv.2510.11479)
- Saha, S., & Sengupta, S. 2021, *AJ*, 162, 221, doi: [10.3847/1538-3881/ac294d](https://doi.org/10.3847/1538-3881/ac294d)
- Saha, S., Jenkins, J. S., Parmentier, V., et al. 2025, *A&A*, 700, A45, doi: [10.1051/0004-6361/202554303](https://doi.org/10.1051/0004-6361/202554303)
- Schneider, A. D., & Bitsch, B. 2021, *A&A*, 654, A71, doi: [10.1051/0004-6361/202039640](https://doi.org/10.1051/0004-6361/202039640)
- Sedaghati, E., Boffin, H. M. J., MacDonald, R. J., et al. 2017, *Nature*, 549, 238, doi: [10.1038/nature23651](https://doi.org/10.1038/nature23651)
- Sedaghati, E., MacDonald, R. J., Casasayas-Barris, N., et al. 2021, *MNRAS*, 505, 435, doi: [10.1093/mnras/stab1164](https://doi.org/10.1093/mnras/stab1164)
- Servoin, J. L., & Piriou, B. 1973, *Physica Status Solidi B Basic Research*, 55, 677, doi: [10.1002/pssb.2220550224](https://doi.org/10.1002/pssb.2220550224)
- Shornikov, S. I. 2019, *Russian Journal of Physical Chemistry A*, 93, 1024, doi: [10.1134/S0036024419060293](https://doi.org/10.1134/S0036024419060293)
- Siefke, T., Kroker, S., Pfeiffer, K., et al. 2016, arXiv e-prints, arXiv:1607.04866, doi: [10.48550/arXiv.1607.04866](https://doi.org/10.48550/arXiv.1607.04866)
- Smith, P. C. B., Sanchez, J. A., Line, M. R., et al. 2024, *AJ*, 168, 293, doi: [10.3847/1538-3881/ad8574](https://doi.org/10.3847/1538-3881/ad8574)

- Sousa-Silva, C., Al-Refaie, A. F., Tennyson, J., & Yurchenko, S. N. 2015, MNRAS, 446, 2337, doi: [10.1093/mnras/stu2246](https://doi.org/10.1093/mnras/stu2246)
- Speagle, J. S. 2020, MNRAS, 493, 3132, doi: [10.1093/mnras/staa278](https://doi.org/10.1093/mnras/staa278)
- Stull, D. R. 1947, Industrial & Engineering Chemistry, 39, 517, doi: [10.1021/ie50448a022](https://doi.org/10.1021/ie50448a022)
- Tumborang, A. A., Spake, J. J., Knutson, H. A., et al. 2024, AJ, 168, 296, doi: [10.3847/1538-3881/ad863f](https://doi.org/10.3847/1538-3881/ad863f)
- Ueda, K., Yanagi, H., Noshiro, R., Hosono, H., & Kawazoe, H. 1998, Journal of Physics Condensed Matter, 10, 3669, doi: [10.1088/0953-8984/10/16/018](https://doi.org/10.1088/0953-8984/10/16/018)
- Weiner Mansfield, M., Line, M. R., Wardenier, J. P., et al. 2024, AJ, 168, 14, doi: [10.3847/1538-3881/ad4a5f](https://doi.org/10.3847/1538-3881/ad4a5f)
- Wiser, L. S., Bell, T. J., Line, M. R., et al. 2025, arXiv e-prints, arXiv:2506.01800, doi: [10.48550/arXiv.2506.01800](https://doi.org/10.48550/arXiv.2506.01800)
- Wong, I., Knutson, H. A., Kataria, T., et al. 2016, ApJ, 823, 122, doi: [10.3847/0004-637X/823/2/122](https://doi.org/10.3847/0004-637X/823/2/122)
- Xue, Q., Bean, J. L., Zhang, M., et al. 2024, ApJL, 963, L5, doi: [10.3847/2041-8213/ad2682](https://doi.org/10.3847/2041-8213/ad2682)
- Zeidler, S., Posch, T., Mutschke, H., Richter, H., & Wehrhan, O. 2011, A&A, 526, A68, doi: [10.1051/0004-6361/201015219](https://doi.org/10.1051/0004-6361/201015219)

APPENDIX

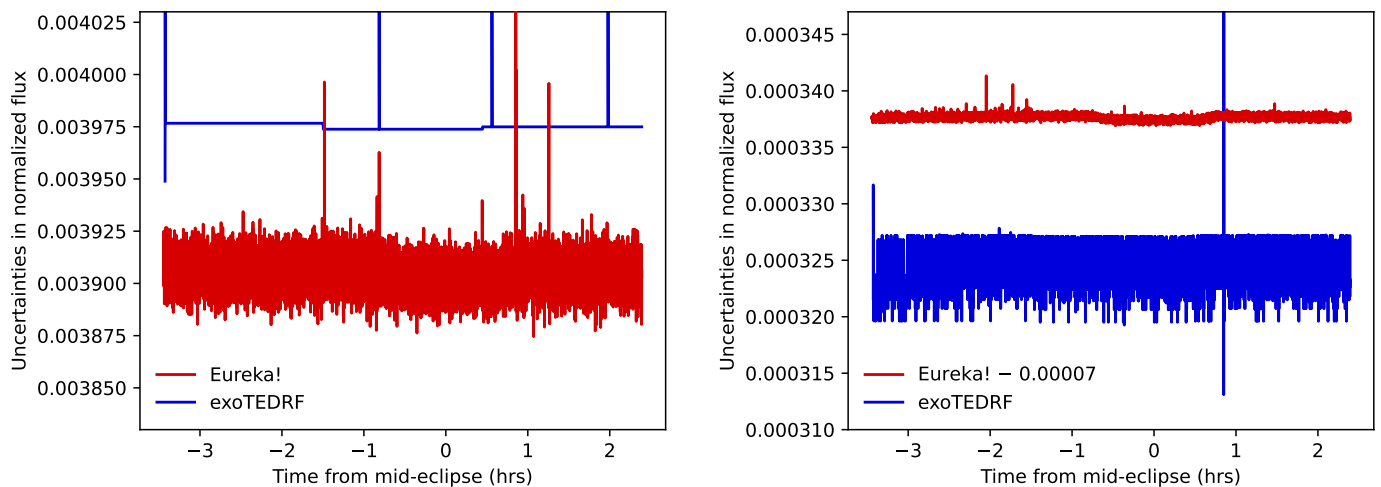


Figure A1. *Left:* Comparison of uncertainties in the 100th spectroscopic lightcurve from Eureka! and exoTEDRF. *Right:* Same comparison for the white lightcurves. exoTEDRF shows mostly constant uncertainties with occasional large fluctuations. In the white lightcurves, the fluctuations dominate, reducing the difference between the two pipelines.

Table A1. Estimated parameters from the white lightcurve fit (Eureka!).

Parameter	Prior	Value
P (days)	fixed	0.788839092
t_0 (MJD)	$\mathcal{N}(59993.01, 0.003)$	$59993.008198 \pm 8.9 \times 10^{-5}$
a/R_*	$\mathcal{N}(3.533, 0.3)$	3.543 ± 0.045
i (deg)	$\mathcal{N}(79.08, 0.3)$	79.56 ± 0.34
R_p/R_*	fixed	0.1441
F_p/F_*	$\mathcal{U}(0, 0.01)$	$0.001725 \pm 1.5 \times 10^{-5}$
e	fixed	0
ω (deg)	fixed	90.0
a_0	$\mathcal{N}(1, 0.005)$	$0.998514 \pm 1.2 \times 10^{-5}$
a_1	$\mathcal{N}(0, 0.0005)$	$-0.000103 \pm 1.1 \times 10^{-5}$
a_2	$\mathcal{N}(0, 0.0005)$	$-0.000267 \pm 1.6 \times 10^{-5}$
a_3	$\mathcal{N}(0, 0.0005)$	$-9 \times 10^{-6} \pm 1.8 \times 10^{-5}$
a_4	$\mathcal{N}(0, 0.0005)$	$4 \times 10^{-6} \pm 1.3 \times 10^{-5}$

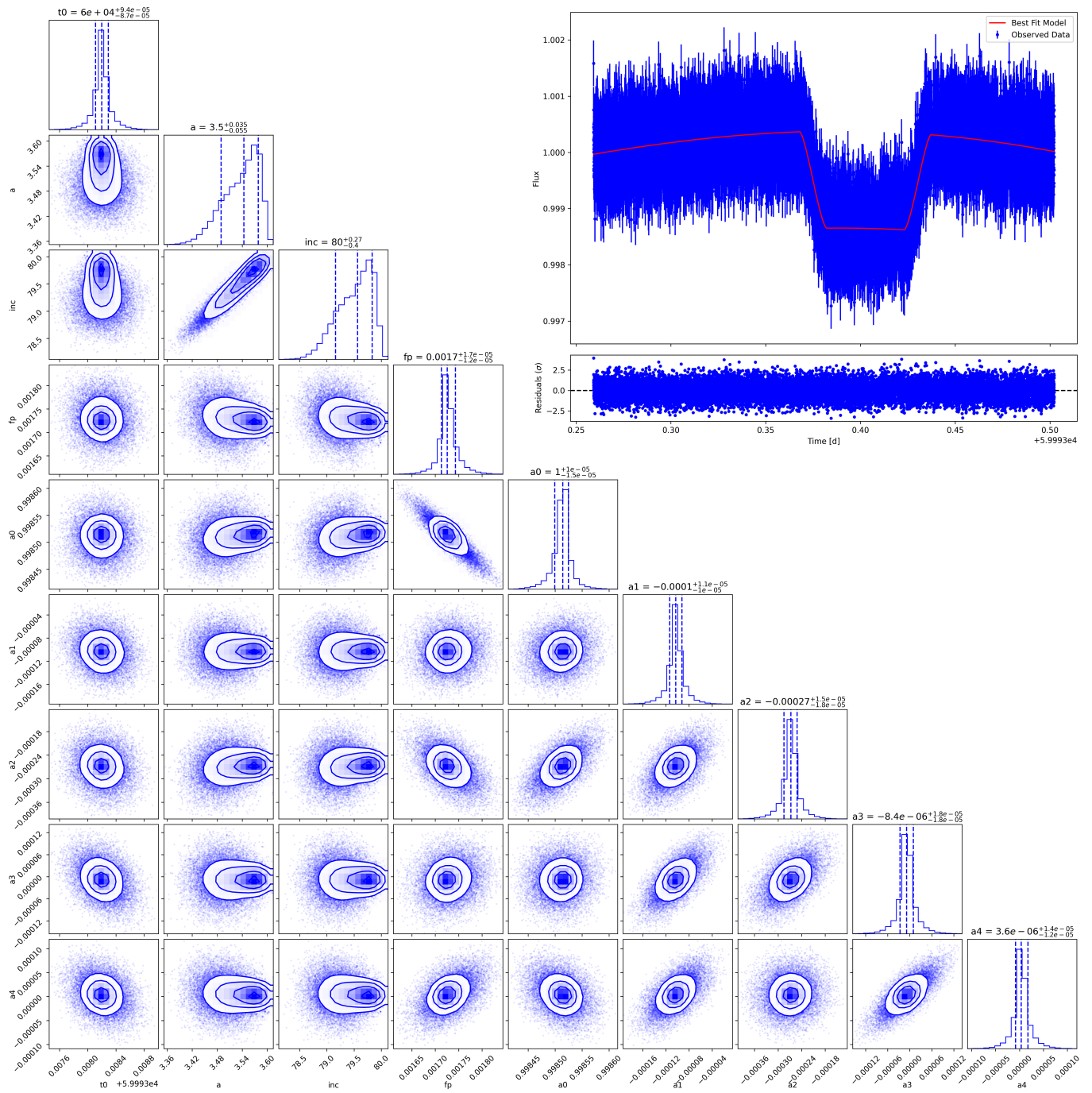


Figure A2. The upper-right panel shows the white lightcurve with the best-fit eclipse model, while the bottom panel displays the corner plot of the model's posterior distribution.

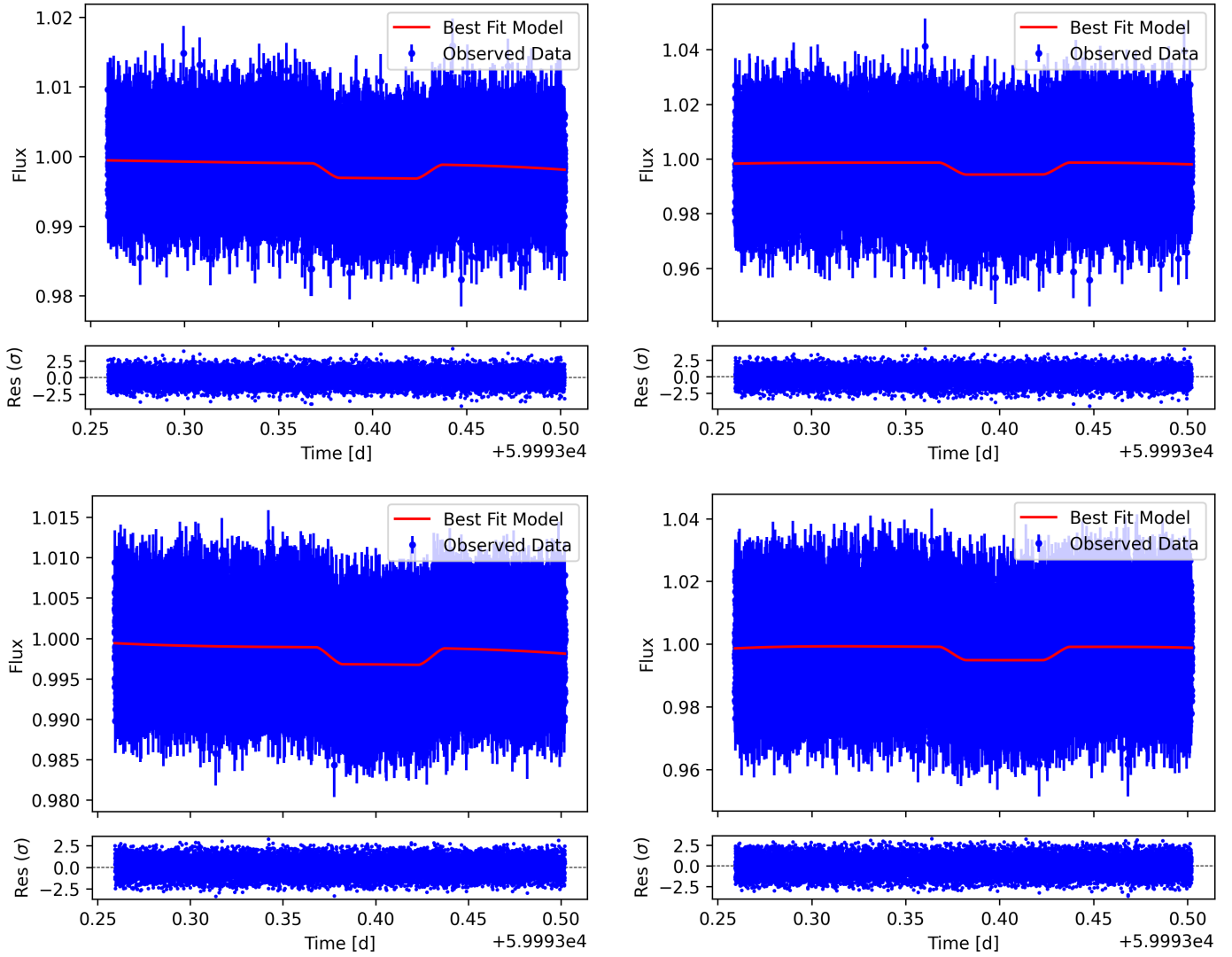


Figure A3. The top two panels show the 100th and 200th spectroscopic lightcurves from the Eureka! reduction with their best-fit eclipse models, while the bottom two panels show the same for the exoTEDRF reduction.

Table A2. Priors of the free parameters used in the atmospheric retrievals.

Parameter	Prior
$T_{\text{int}[K]}$	$\mathcal{U}(0, 1000)$
$T_{\text{equ}[K]}$	$\mathcal{U}(0, 5000)$
$[\gamma]$	$\mathcal{U}(-2, 2)$
$[\kappa_{\text{IR}}]$	$\mathcal{U}(-4, 0)$
f_{sed}	$\mathcal{U}(0.1, 20)$
σ_{Inorm}	$\mathcal{U}(1, 5)$
$[K_{zz}]$	$\mathcal{U}(2, 15)$
f_c	$\mathcal{U}(0, 1)$
$[Z/Z_{\odot}]$	$\mathcal{U}(-2, 2)$
C/O	$\mathcal{U}(0.05, 2)$
$[P_q]$	$\mathcal{U}(-12, 2)$
$[\text{H}_2\text{O}]$	$\mathcal{U}(-12, -0.5)$
$[\text{CO}]$	$\mathcal{U}(-12, -0.2)$
$[\text{CO}_2]$	$\mathcal{U}(-12, -0.5)$
$[\text{SiO}]$	$\mathcal{U}(-12, -0.2)$
$[\text{CH}_4]$	$\mathcal{U}(-12, -1.0)$
$[\text{C}_2\text{H}_2]$	$\mathcal{U}(-12, -1.0)$
$[\text{HCN}]$	$\mathcal{U}(-12, -1.0)$
$[\text{PH}_3]$	$\mathcal{U}(-12, -1.0)$
$[\text{H}_2\text{S}]$	$\mathcal{U}(-12, -1.0)$
$[\text{TiO}]$	$\mathcal{U}(-14, -1.0)$
$[\text{VO}]$	$\mathcal{U}(-14, -1.0)$
$[\text{MgSiO}_3(\text{s})]$	$\mathcal{U}(-14, -0.2)$
$[\text{Mg}_2\text{SiO}_4(\text{s})]$	$\mathcal{U}(-14, -0.2)$
$[\text{Al}_2\text{O}_3(\text{s})]$	$\mathcal{U}(-14, -0.2)$
$[\text{SiO}_2(\text{s})]$	$\mathcal{U}(-14, -0.2)$
$[\text{CaTiO}_3(\text{s})]$	$\mathcal{U}(-14, -0.2)$
$[\text{TiO}_2(\text{s})]$	$\mathcal{U}(-14, -0.2)$

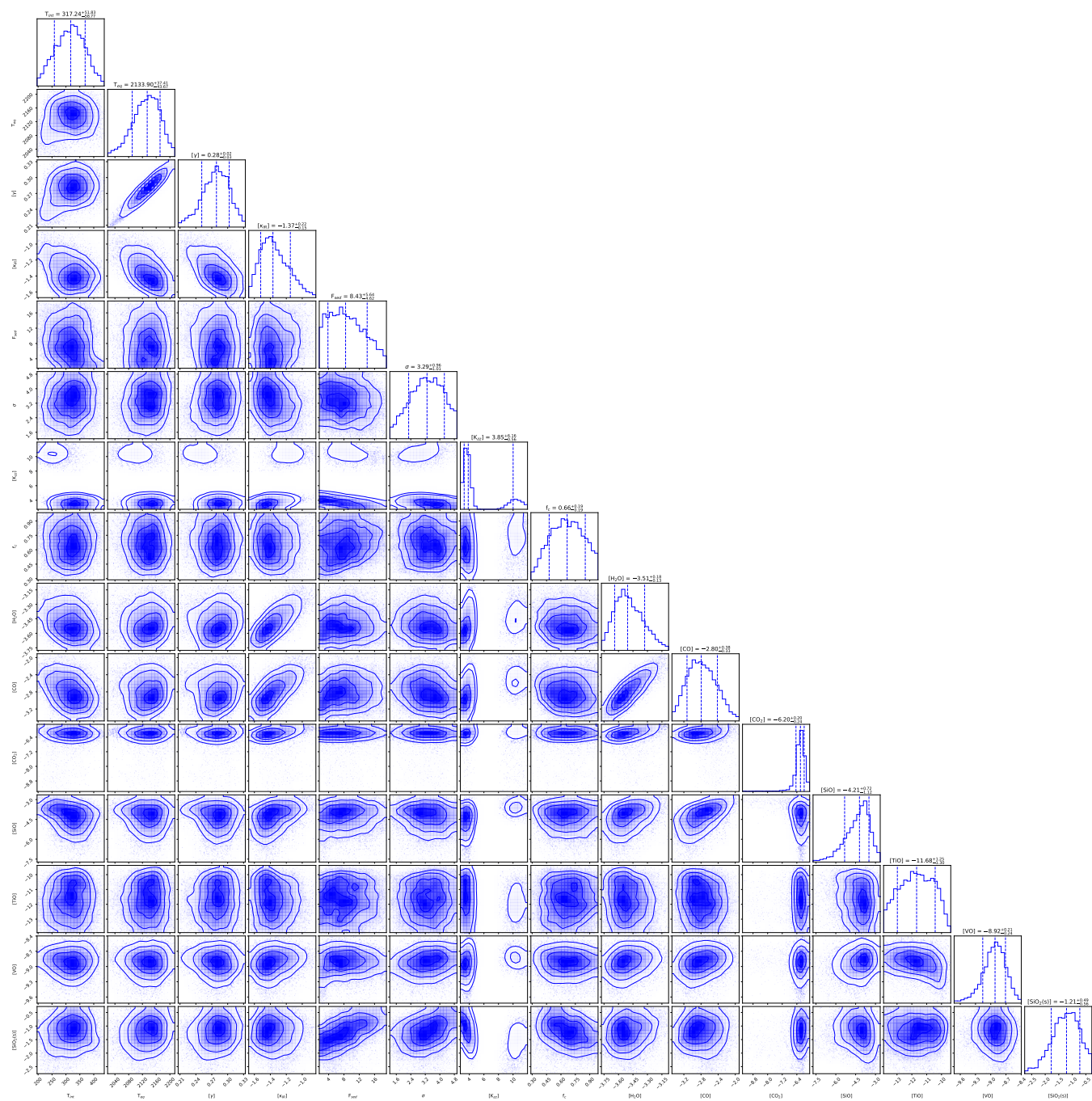


Figure A4. Corner plot showing the posterior distributions from the free chemistry retrieval analysis (Eureka!), including only the well-constrained molecular species.

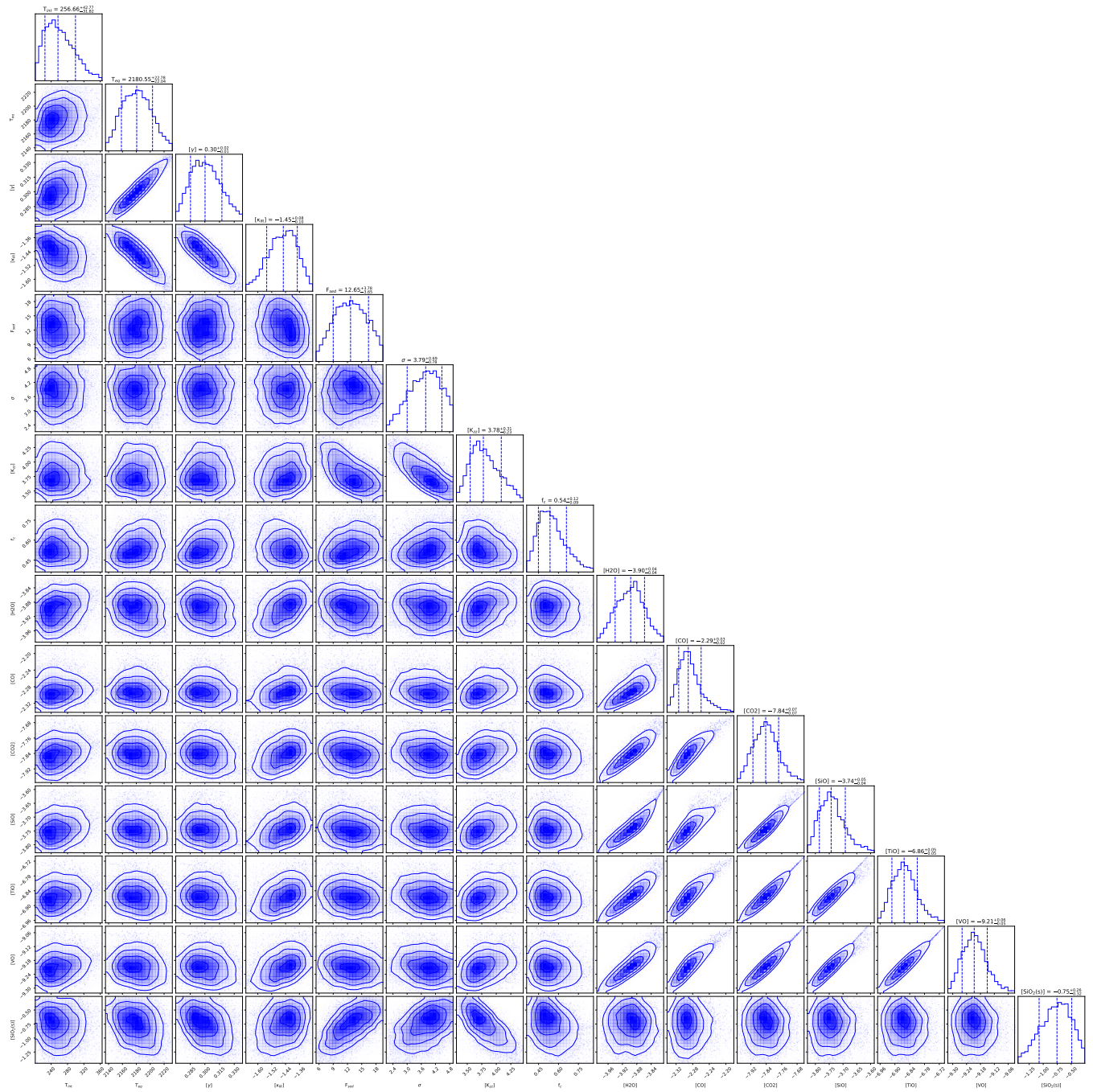


Figure A5. Same as Figure A4, but for the equilibrium chemistry retrieval.

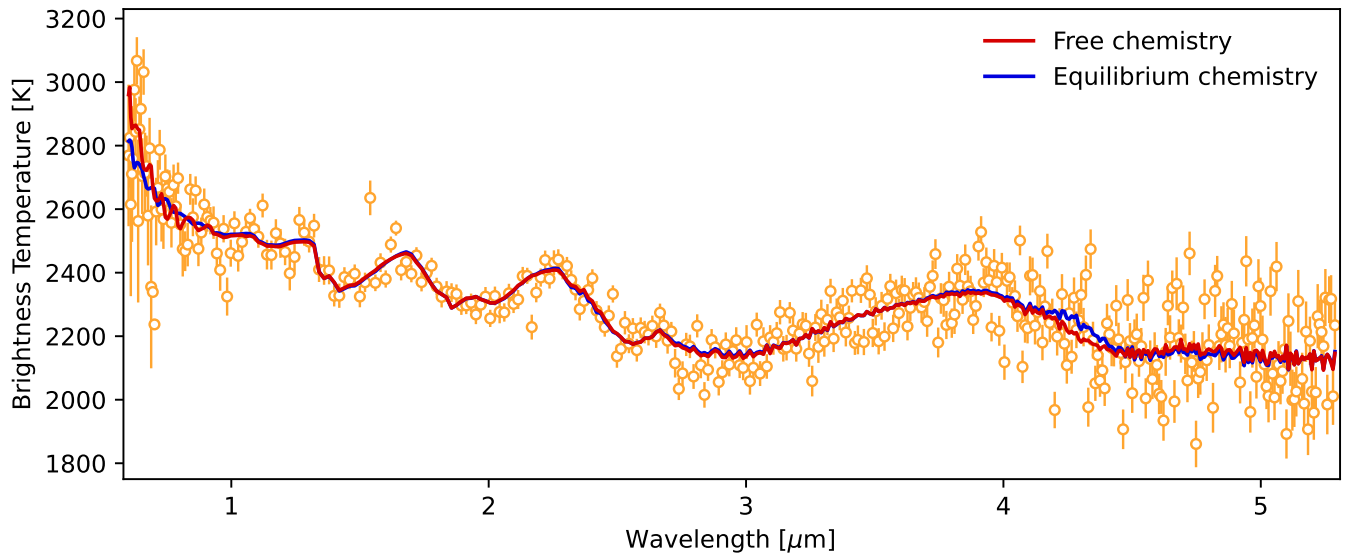


Figure A6. The observed emission spectrum of WASP-19b (Eureka!, orange), shown alongside the best-fit free and equilibrium chemistry models, demonstrating strong consistency.

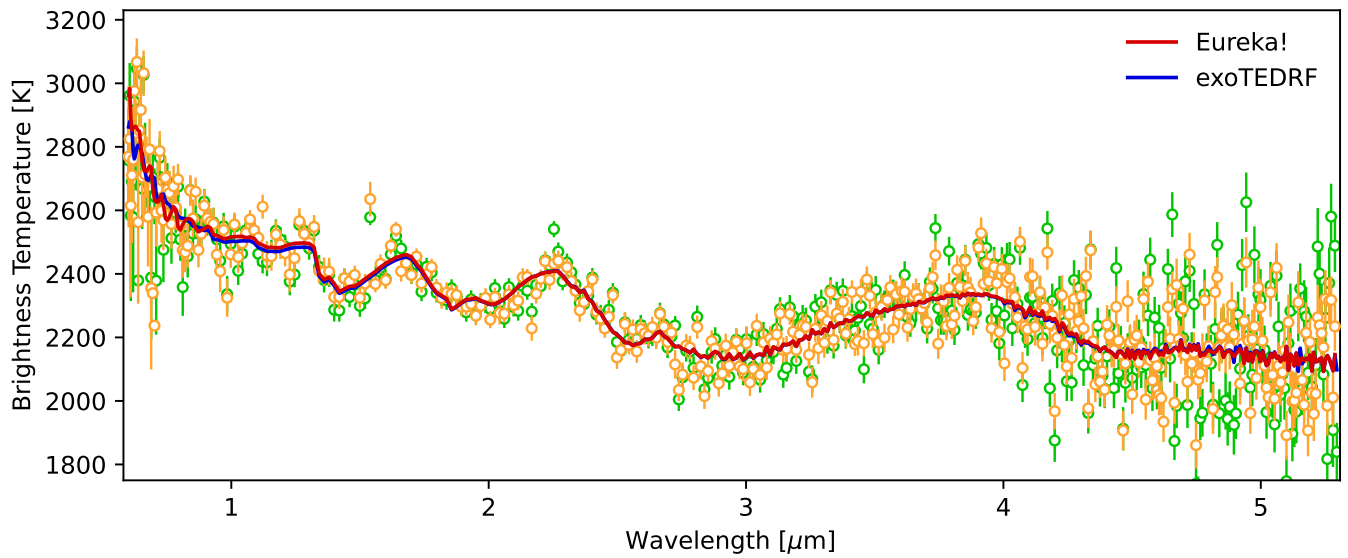


Figure A7. The observed emission spectra of WASP-19b from both Eureka! (orange) and exoTDRF (green) are shown alongside their corresponding best-fit free chemistry models. Both models show strong consistency, validating the robustness of retrieved properties.